American Mineralogist, Volume 84, pages 1932–1938, 1999

Mottled contrast in TEM images of mica crystals

DAVID CHRISTOPHER NOE* AND DAVID R. VEBLEN

Department of Earth and Planetary Sciences, The Johns Hopkins University, Baltimore, Maryland 21218, U.S.A.

ABSTRACT

Mottling in [*uv*0] micrographs is a common feature of phyllosilicates observed with transmission electron microscopes and has been attributed to various mechanisms. The similar appearance of the mottling among various samples suggests that it arises from a common mechanism. Diffraction-contrast experiments demonstrate that it is caused by variations in basal plane spacings. A second type of mottling was identified that has not been previously described. This mottling is most apparent in dark-field images obtained with the electron beam oriented approximately normal to the basal plane, but the mechanism responsible for this mottling could not be determined. Both types of mottling occur as primary features but can be affected or even created by beam-induced changes. The induced nature of some mottling suggests that caution should be used when interpreting mottled features.

INTRODUCTION

Mottling in TEM images of phyllosilicates is common and has been described by numerous previous investigators. A relationship between mottling and defects such as microcleavages and phase boundaries has been noted and generally attributed to strain contrast (Livi et al. 1997; Merriman et al. 1995; Jiang and Peacor 1993; Livi and Veblen 1987). Mottling has also been attributed to beam damage (Shau and Peacor 1992; Ahn et al. 1986), exsolution effects (Ferrow et al. 1990), Guinier-Preston zones (Page 1980), and "destabilized states" (De Parseval et al. 1994).

This study considers two different types of mottling. The first type is visible in micrographs that have an end-on view of the (001) basal planes and is here referred to as type 1 mottling. The second (type 2 mottling) has not previously been described and is best seen in dark-field (DF) images viewed normal to the basal planes. A combination of high-resolution TEM (HRTEM), selected-area electron diffraction (SAED), analytical electron microscopy (AEM), and electron microprobe analysis (EMP) has been used. Our goal is to determine if mottling is a primary feature or if it results from sample preparation or beam damage for this important group of minerals.

EXPERIMENTAL TECHNIQUES

Phyllosilicate crystals were selected for analysis from the Williams research collection at the Johns Hopkins University Department of Earth and Planetary Sciences, the U.S. National Museum of Natural History, and private collections. Data on sample localities and sources are in Table 1.

Crushed-grain mounts were prepared by grinding small cleavage flakes in an agate mortar and suspending the resultant powder in ethanol or water before deposition onto a holey carbon grid. The grinding process was of concern due to the possibility of deformation-produced features. A comparison of powder mounts and cleavage flakes from identical localities indicated that the features of concern were present in both types of samples. The risk of introducing mottling from grinding therefore appears to be small.

Cleaved samples were prepared by gluing small cleavage flakes to copper washers (hole grids) and splitting them with adhesive tape or a razorblade until the samples were thinner than approximately 30 μm. A few of these samples were then ion milled; other samples were further split until small holes were produced. The regions around these holes were extremely thin and did not display the characteristic amorphization produced by ion milling.

A few specimens were prepared by embedding pieces in epoxy and thin sectioning. This method was used for the preparation of samples to be imaged parallel to the cleavage planes. These specimens were then thinned by argon-ion milling.

TEM and AEM

All samples were examined in the Philips 420ST TEM in the Johns Hopkins University Department of Earth and Planetary Sciences. The instrument was operated at 120 keV and analytical data were collected using an energy dispersive spectroscopy (EDS) system with an Oxford Analytical detector and Princeton Gamma-Tech System IV spectrum analyzer. The data were treated as described by Livi and Veblen (1987).

Electron microprobe analyses

EMP analyses (Table 2) were acquired with the JEOL 8600 Superprobe located in the Johns Hopkins University Department of Earth and Planetary Sciences. Quantitative analyses were obtained with a circular, approximately 5 mm, 15 keV, 20 nA beam. Standards used were albite for Na; enstatite for Mg; anorthite for Al, Si and Ca; orthoclase for K; anatase for Ti; rhodonite for Mn; fayalite for Fe; and fluorphlogopite for F. Data reduction was performed with the CITZAF program (Armstrong 1989).

*Current address: 11860 Wilshire Dr., N. Huntingdon, PA 15642, U.S.A. E-mail: Noed@hwr.com

TABLE 1. Sample information

Mineral	Locality	Notes	Source
Biotite	Ruby Mountain Mylonite, Utah	Samples prepared from small samples of biotite "fish"*. prepared from thin sections both parallel and perpendicular to the foliation plane.	Private Collection (A. Snoke)
	Bancroft, Ontario	Thin sections, cleavage flakes, crushed grain mounts.	Wards Catalog
	Russia	Crushed-grain mounts.	NMNH no. 103149
Clintonite	Achmatovsk, Urals	Xanthophyllite variety. Thin sections, cleavage flakes, crushed grain mounts.	Williams 465.A2-A
	Amity, N.Y.	Sybertite variety. Thin sections, crushed grain mounts.	Williams 465.1-A
Margarite	Chester, Mass.	Crushed grain mounts.	Williams 464-C
Muscovite	Paris, Maine	Crushed grain mounts	Williams 458.2-P2
Phlogopite	St. Lawrence County, N.Y.	Crushed grain mounts.	Williams 462a-S

* Biotite "fish" are a texture produced during intense shearing (Hurlow et al. 1991; Lister and Snoke 1984).

TABLE 2. EMP data

	Si	Al (total)	Al IV	Al VI	Cr	Ti	Fe^{2+}	Mg	Mn	Ca	Na	K	F	H
Clintonite A	1.20	3.53	2.80	0.73	0.00	0.00	0.14	2.15	0.00	1.00	0.00	0.00	0.00	2.00
Clintonite B	1.35	3.31	2.65	0.67	0.00	0.02	0.11	2.20	0.00	0.98	0.01	0.00	0.37	1.63
Biotite (Bancroft)	3.06	.092	0.94	0.00	0.00	0.12	0.71	2.05	0.01	0.00	0.06	0.94	1.03	0.97
Biotite (NMNH 103149)	2.74	1.71	1.26	0.45	0.00	0.12	1.28	0.93	0.02	0.00	0.01	0.94	0.02	1.98

Notes: Average of five analyses. Normalized to Σ(F, OH) = 2. All Fe assumed to be Fe^{2+}.

RESULTS

Type 1 Mottling

Type 1 mottling consists of large, "blocky" patches and smaller, irregular areas of darker contrast that commonly terminate against basal planes (Fig. 1). It is similar in appearance to features produced by diffraction contrast in strained areas of a crystal. Mottling of a similar appearance was reported in several studies (Livi et al. 1997; Merriman 1995; De Parseval 1994; Jiang and Peacor 1993; Shau and Peacor 1992; Livi and Veblen 1987; Ahn et al. 1986; Page 1980), which suggests that the underlying strain properties may be similar in most of the observed crystals. Because strain produces diffraction contrast, an analysis of Bragg's Law may offer insights to the origin of the mottling. The wavelength of electrons is constant, so the two variables of concern are d, the spacing between diffracting planes, and θ, the angle between incident electrons and the diffracting planes (changes in θ occur from localized rotation of diffracting planes away from perfect orientation; the axis about which rotation has occurred will be denoted as φ). DF microscopy can be used to help to distinguish between the effects of the two variables. If mottling arises from a change in θ, then contrast will only be changed if φ is not normal to the diffraction vector, $\boldsymbol{g}$. If the φ and $\boldsymbol{g}$ are normal, then $\boldsymbol{g}\cdot\boldsymbol{R} = 0$, and the mottling should not be observable (where $\boldsymbol{R}$ is the defect displacement vector). The DF images indicate that the mottling is not observable for diffraction vector 200 (Fig. 2), so the rotation axis would have to be parallel to $\boldsymbol{a}$*. Mottling is also not visible for $\boldsymbol{g} = 020$, requiring that φ be parallel to $\boldsymbol{b}$*. Because both criteria cannot be fulfilled simultaneously, mottling does not arise from large changes in θ.

Changes in d could result from changes in the basal plane spacing, lateral contractions, or both. The observation that $\boldsymbol{g}\bullet\boldsymbol{R} = 0$ for $\boldsymbol{g} = h00$ and $\boldsymbol{g} = 0k0$ reflections, however, indicates that $\boldsymbol{R}$ is parallel to $\boldsymbol{c}$*, and is probably related to expansion or contraction of the basal planes. Ahn et al. (1986) described a contraction in $\boldsymbol{c}$ due to electron-beam exposure of paragonite, and a consequent splitting of interlayer regions into microcleavages; this was attributed to loss of Na in the interlayer cation position and consequent collapse of the structure. Although not the same as type 1 mottling, these microcleavages represent local-

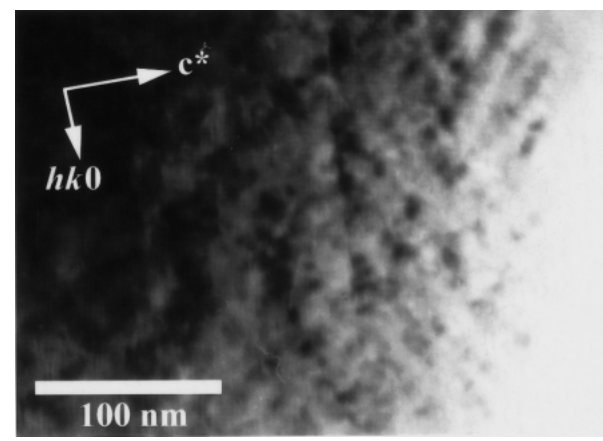

FIGURE 1. Bright-field TEM image of type 1 mottling in an unstrained crystal of Bancroft biotite.

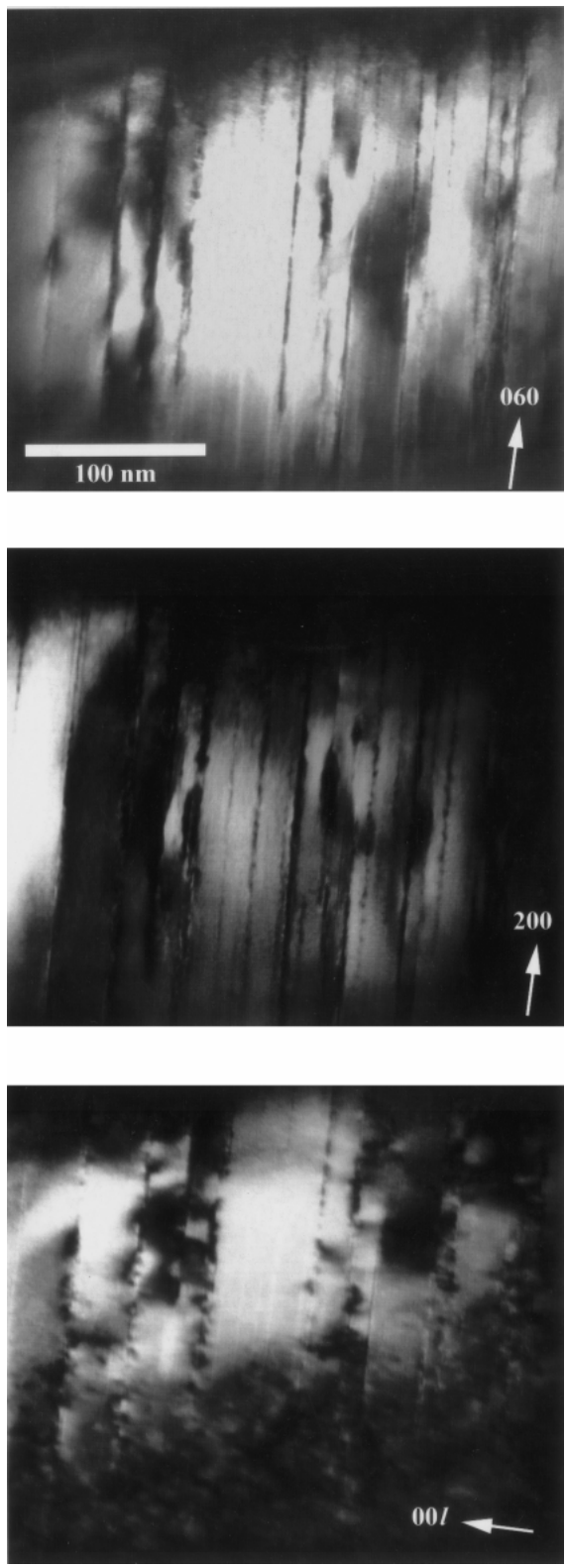

FIGURE 2. Dark-field images of type 1 mottling. Note the "birds eye" mottling present in the bottom image. Images formed with 00*l* diffraction vectors contain a type of contrast not found with *hk*0 diffraction vectors.

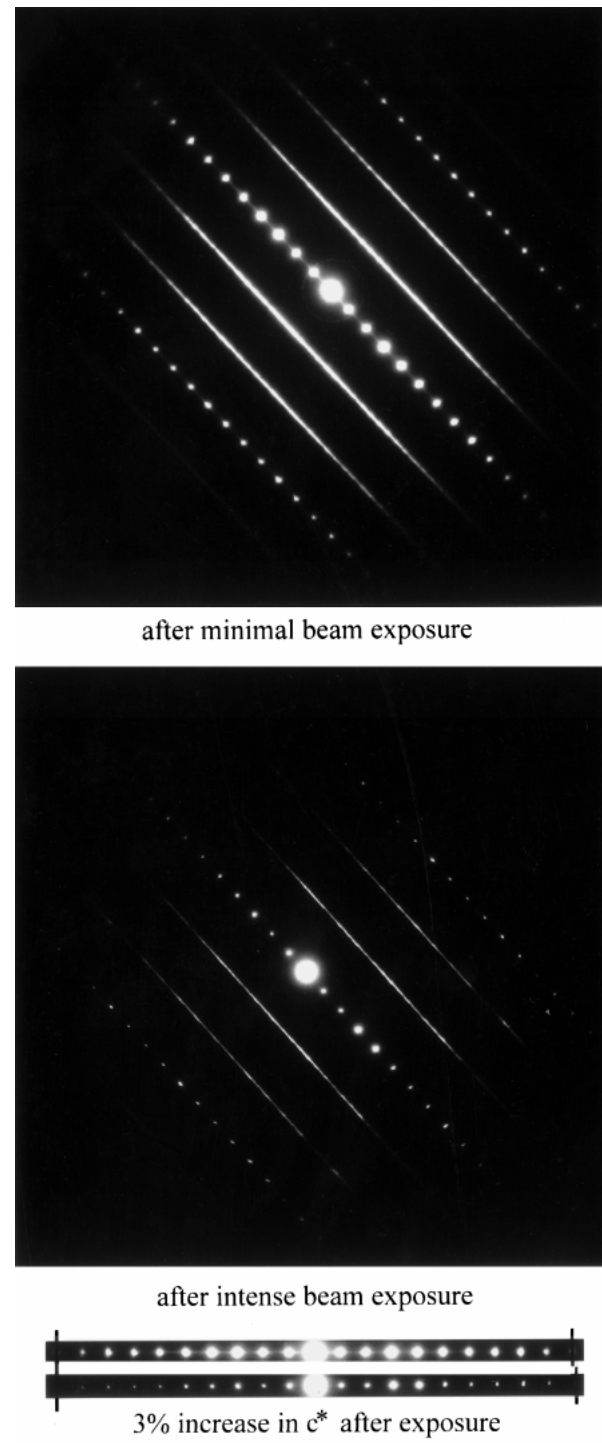

FIGURE 3. Exposure to the electron beam results in an increase of the c* axial length. The bottom portion displays differences in the 00l row between the two diffraction patterns; note the offset between lines on the right-hand side. These patterns were taken before and after images in Figure 4.

ized parting of basal planes. Intense exposure also produces both a reduction in d_{001} (expansion of $\boldsymbol{c}^*$) by approximately 3% (Fig. 3) and occasional microcleavages in the samples used in this study. This suggests that mottling results from localized interlayer collapse. It is not clear whether such mottling can also be a primary feature. Although it is present in most samples immediately upon observation, samples that have not previously been exposed to the beam could perhaps display this mottling after the minimal exposure required for orientation. Chemical analyses of phyllosilicates commonly indicate alkali cation concentrations that are less than one atom per formula unit (Guidotti 1984); if the implied vacancies are heterogeneously distributed, then collapsed areas (and mottling) may be original features. In addition to microcleavages, intense exposure to the electron beam also produces a reduction in the intensity and distribution of type 1 mottling (Fig. 4). This is probably due to the expansion of microcleavages from small, localized features to large, continuous fractures; these fractures may reduce the localized strain responsible for type 1 mottling.

Type 2 mottling

Type 2 mottling is most apparent in DF images formed with $\boldsymbol{g} = h00$, $\boldsymbol{g} = 0k0$, or $\boldsymbol{g} = hk0$ diffraction vectors (Fig. 5). It consists of short, curvey lines that commonly intersect with other lines or terminate. It sweeps about chaotically during sample rotation and does not remain fixed to one area of the sample. It is insensitive to changes in defocus, but the contrast can move due to changes in beam deflection.

Type 2 mottling does not seem to have a consistent defect vector associated with it. Although type 2 mottling is present in DF images formed with the six non-equivalent $0k0$, $h00$, $hh0$, $h\bar{h}0$, $3h\ h\ 0$, and $3h\bar{h}0$ diffraction vectors, specific mottled features generally could not be matched between the micrographs, even though they were collected from the same area and have identifiable morphological features. Rotation of the sample away from an aligned zone axis is required for a two-beam approximation, but rotation was found to change the appearance of type 2 mottling. For this reason, some sets of DF images were formed from aligned zone axes without rotation. Two-beam conditions were not well approximated in these micrographs, but the sample did not require rotation, and it was hoped that mottling could be correlated between micrographs (Fig. 6). Unfortunately, mottling still could not be matched between micrographs. Type 2 mottling is not apparent in images formed with $\boldsymbol{g} = 00l$, indicating that if the mottling does have a defect vector associated with it, it does not have a substantial component parallel to $\boldsymbol{c}^*$. Because type 1 mottling does arise from a defect vector parallel to $\boldsymbol{c}^*$, type 1 and type 2 mottling probably result from different types of structural imperfections.

Crystals oriented to display type 2 mottling in DF mode also display a curious mottled appearance in BF mode (Fig. 7). This mottling is most apparent for orientations in which intensities in the $h00$ row of reflections are maximized. Using a medium-sized objective aperture (47 μm) results in images that have patches of contrast both lighter and darker than the surrounding structure; using a small objective aperture that is only slightly larger than the transmitted beam (2.5 μm) results in

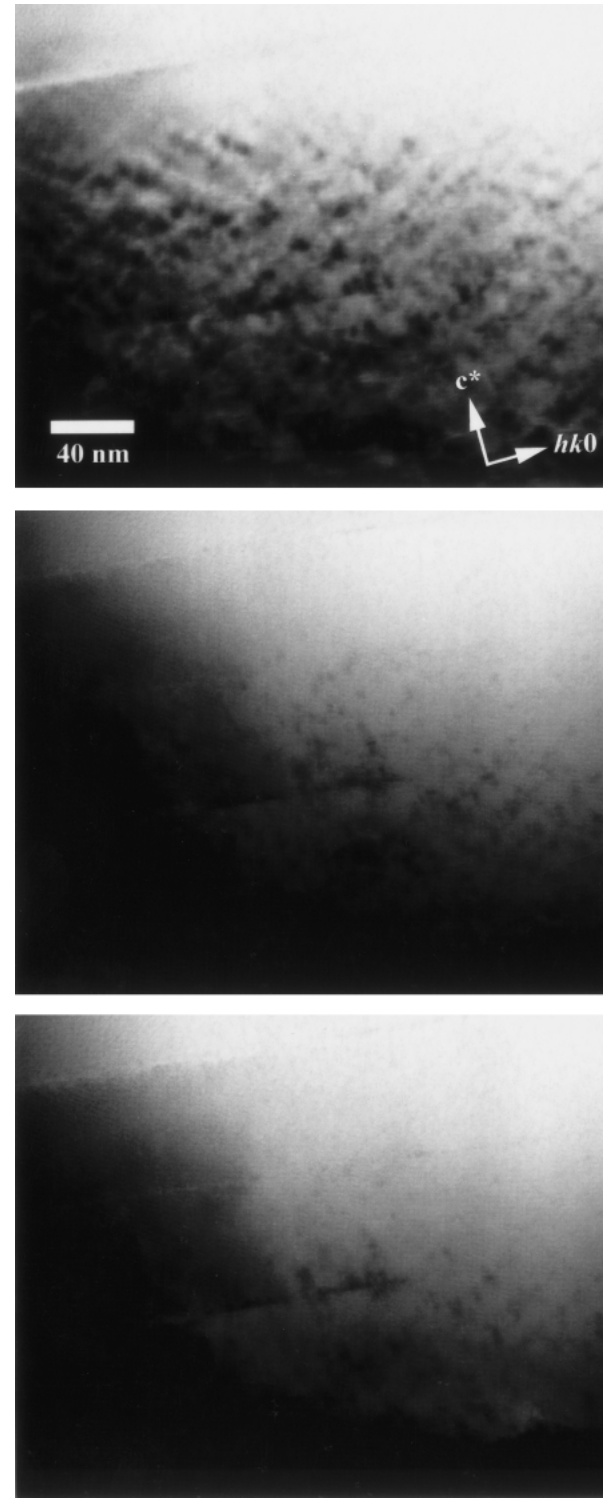

FIGURE 4. Time-series bright-field micrographs demonstrating the effect of beam exposure on type 1 mottling. The top micrograph was taken after minimal beam exposure; approximately two minutes of intense exposure separates the following micrographs. Note the significant decrease in mottling with time, particularly between the first and second micrographs.

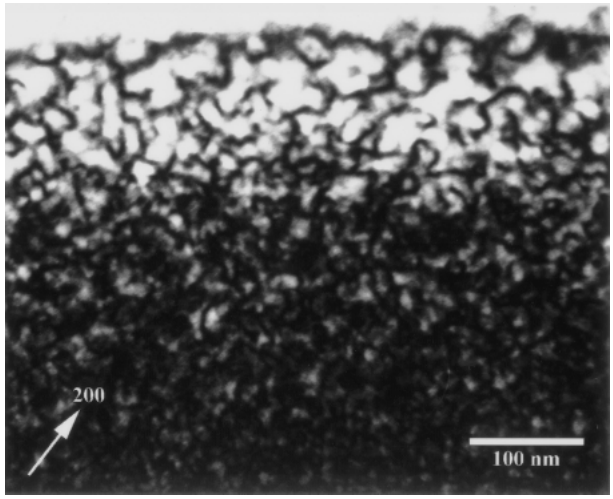

FIGURE 5. Type 2 mottling in a dark-field image from an unstrained crystal of Bancroft biotite. The crystal was not mylonitized or ion milled, indicating that type 2 mottling is not a product of these processes.

images that contain patches of dark contrast without the light contrast. This suggests that the darker patches arise from diffraction contrast. As with the DF images, the mottling displays chaotic changes during sample rotation.

If type 2 mottling does arise from diffraction contrast effects, then it may be related to short range ordering (SRO) in crystals. Diffuse scattering in crystals with SRO can produce DF images that have a speckled appearance (Kudoh et al. 1993; Cowley 1972). Speckling in the DF images of Kudoh et al. (1993) and Cowley (1972) is on the length scale of a few tenths of nanometers (type 2 mottling has a length scale of a few nanometers), and does not display well-resolved curvilinear features. In addition, the SAED patterns from crystals used in this study do not display obvious diffuse scattering. It cannot be ruled out, however, that type 2 mottling is related to extremely diffuse scattering that is not apparent in the SAED patterns. The curved line segments in DF images of type 2 mottling are somewhat similar to images of dislocation networks, but the chaotic changes in mottling with rotation are not consistent with type 2 mottling being dislocation networks. In addition, several of the line segments can be seen to terminate, which is not possible for dislocations unless they intersect a crystal surface. Because dislocations in phyllosilicates are generally confined to the basal planes (except for growth spirals), they cannot encounter the top or bottom of samples in this orientation and cannot produce the terminal segments.

Type 2 mottling was first noticed in the mylonitic samples that had been heavily deformed and should contain abundant dislocations. As a second check of whether the mottled contrast or curvy line segments are deformation features, samples were prepared from crystals of biotite from Bancroft, Ontario. These samples were of igneous or metasomatic origin and exhibit no features indicative of deformation. Samples were prepared by cutting small flakes from a large crystal with a razorblade and then gluing these flakes to copper grids. In most cases, samples were then ion milled to determine if type 2 mottling was produced by damage in the ion mill. A sample was also prepared by gluing a small biotite flake to a copper grid and then cleaving the flake with a razorblade until it was thin enough for use in the TEM (without ion milling). TEM analysis of these crystals revealed type 2 mottling similar to that in other samples.

To determine whether or not type 2 mottling was unique to biotite, samples of muscovite, phlogopite, margarite, and clintonite were examined. Type 2 mottling was readily apparent in the muscovite and phlogopite samples. In both margarite samples, type 2 mottling became more intense with beam exposure. Samples were observed to progress from a nearly mottle-free state to an extremely high density of mottling when an intense beam was left on the sample for a few minutes. Clintonite was even more interesting. Samples from the Williams 465A2-A specimen did not develop either type 1 or type 2 mottling with exposure. Samples from the 465-1A specimen did develop mottling with exposure, similar to the margarite specimens. The difference in behavior between clintonite specimens provided an opportunity to correlate the appearance of type 2 mottling with composition.

AEM analyses were collected for the clintonite, margarite, mylonitic biotite, and Bancroft biotite specimens (Table 3), and EMP data (Table 2) were collected for selected biotite and clintonite specimens. The limited number of samples used in this study restricts the conclusions that can be made. However, the biggest difference in composition between the clintonite samples involves F content. Fluorine was detected in all of the samples analyzed, except for the clintonite specimen that did not display type 2 mottling (Williams 465A2-A). To determine if F is related to the presence of mottling, samples of biotite with a very low concentration of F (NMNH no. 103149) were observed in the TEM. Type 2 mottling was readily apparent in these samples, indicating that F is probably not the only chemical variable responsible for mottling. The clintonite specimens without mottling also have a higher Al/Si ratio (2.94) than the samples with mottling (2.30). It is not known whether Al/Si influences type 2 mottling.

DISCUSSION

Type 1 mottling

Numerous studies have reported mottled contrast identical in appearance to the type 1 mottling imaged in this study, sug-

TABLE 3. AEM analyses

	Si	Al	Ti	Fe	Mg	Mn	Ca	Na	K	Cu	Mo
Clintonite A (Will. 465.A2-A)	1.00	2.30	0.01	0.13	1.42	0.00	0.78	0.08	0.01	0.00	0.00
Clintonite B (Will. 465.1-A)	1.00	2.02	0.02	0.08	1.20	0.00	0.57	0.04	0.01	0.00	0.00
Margarite (Will. 470C)	1.00	1.95	0.01	0.04	0.02	0.00	0.37	0.13	0.03	0.00	0.00
Biotite (Ruby Mountain)	1.00	0.54	0.04	0.40	0.26	0.01	0.03	0.04	0.21	0.00	0.00
Biotite (Bancroft)	1.00	0.32	0.05	0.28	0.62	0.00	0.00	0.32	0.43	0.00	0.00

Notes: Average of three analyses. Normalized to 1 Si.

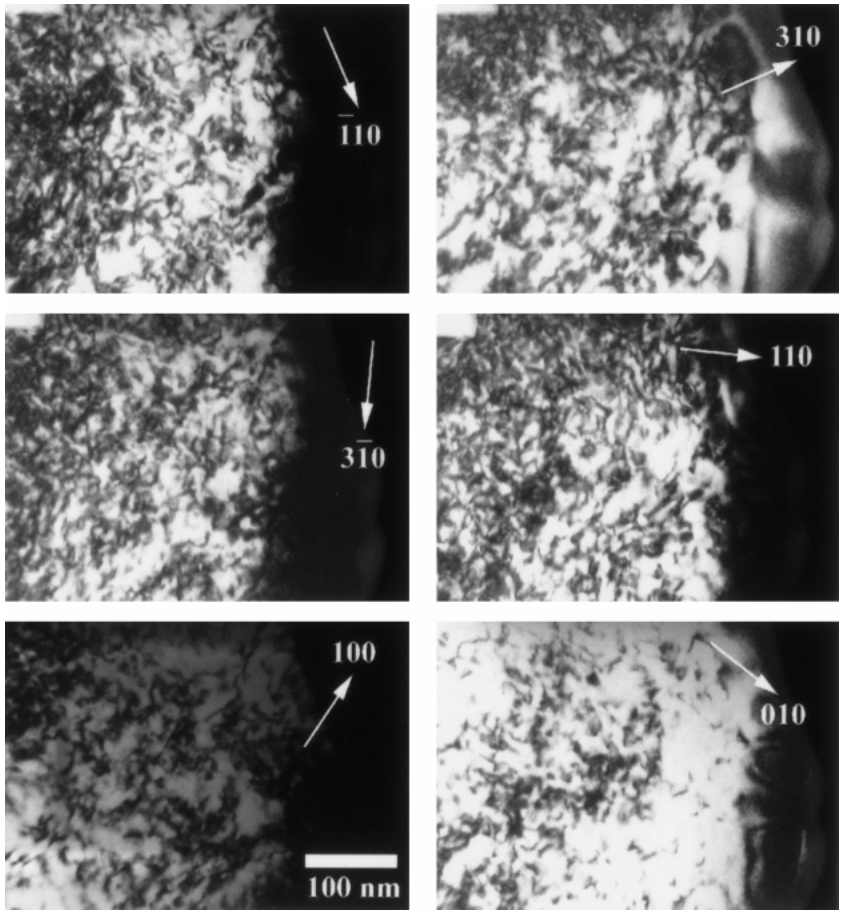

FIGURE 6. Dark-field images for both sets of pseudo-equivalent axes in biotite. To facilitate comparison between the images, an aligned *hk*0 diffraction pattern was used, and the crystal was not rotated between exposures. The mottling does not disappear completely with any of the diffraction vectors, although it does change unpredictably. The scale bar in the lower right is 100 nm.

gesting that it may arise from similar mechanisms. The evidence shows that it is due to variations in the basal plane spacing; these variations have been shown to result from sample-beam interactions. The presence of type 1 mottling in some specimens after minimal beam exposure indicates that it may have a primary origin in some cases. The spacing variations arise from small partings along cleavage planes or from chemical heterogeneity. The underlying cause is probably chemical heterogeneity in the interlayer. Likely primary and secondary causes involve local clustering of vacancies or interlayer cations; in the primary case these are original features and in the secondary case they arise from beam-induced diffusion.

Type 2 mottling

Terminal line segments and the chaotic changes in appearance upon rotation indicate that type 2 mottling does not arise from dislocations. Rapid changes in line position can occur upon rotation for Moiré patterns and bend contours. Because the appearance of mottling remains constant with changes in defocus, however, Moiré patterns are probably not responsible. Bend contours are also unlikely. Type 2 mottling is manifested as darker-contrast lines on a light background (in DF mode), indicating that the crystal is generally in a strong diffracting condition. If the lines resulted from small, localized bends that are not in a strong diffracting condition, then the position of lines should remain relatively invariant upon rotation.

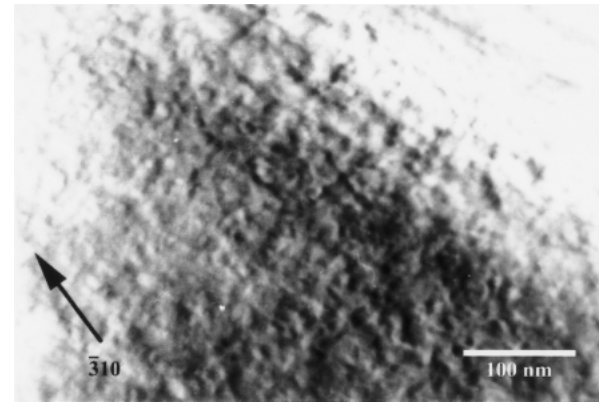

FIGURE 7. Type 2 mottling in a bright-field image from an unstrained crystal of Bancroft biotite. This image was formed from an *hk*0 diffraction pattern that was rotated off-center to emphasize the 310 row of reflections.

The similarities between type 2 mottling and DF images of SRO in crystals warrants further investigation. The curvilinear lines in Figures 5 and 6 grade into areas with a higher density

of mottling, and these areas appear somewhat similar to the DF images of Kudoh et al. (1993) and Cowley (1972). The areas with obvious curvilinear lines may represent thinner regions in the samples used in this study. The lack of obvious diffuse scattering in the SAED patterns is difficult to account for with this interpretation, but no quantitative studies have been performed on the SAED intensities. TEM investigation with a high-resolution electron energy-loss spectroscopy (EELS) system (not available on the Philips 420ST used in this study) might reveal the presence of small-scale chemical segregations that could be responsible for SRO and type 2 mottling in mica samples. In particular, it would be interesting to determine if Al-Si segregation occurs on a small scale. Al-Si ordering could also be a factor, but would not be easily detectable.

ACKNOWLEDGMENTS

Financial support for this study was provided by NSF grant EAR-9418090 to David R. Veblen. This manuscript was improved by reviews from J. Hughes, J. Ferry, D. Peacor, and D.R. Peavar.

REFERENCES CITED

Ahn, J.H., Peacor, D.R., and Essene, E.J. (1986) Cation-diffusion-induced characteristic beam damage in transmission electron microscope images of micas. Ultramicroscopy, 19, 375–382.

Armstrong, J.T. (1989) CITZAF: Combined ZAF and Phi-rho (Z) Electron Beam Correction Programs. California Institute of Technology, Pasadena, CA.

Cowley, J.M. (1973) High-resolution dark-field electron microscopy. II. Short-range order in crystals. Acta Crystallographica, A29, 537–540.

De Parseval, P., Amouric, M., Baronnet, A., Fortune, J-P., Moine, B., and Ferret, J. (1994) HRTEM study of the chloritization of micas in the talc-chlorite deposit at Trimouns (Pyrenees, France). European Journal of Mineralogy, 6, 123–132.

Ferrow, E.A., London, D., Goodman, K.S., and Veblen, D.R. (1990) Sheet silicates of the Lawler Peak granite, Arizona: chemistry, structural variations, and exsolution. Contributions to Mineralogy and Petrology, 105, 491–501.

Guidotti, C.V. (1984) Micas in metamorphic rocks. In Mineralogical Society of America Reviews in Mineralogy, 13, 357–468.

Hurlow, H.A., Snoke, A.W., and Hodges, K.V. (1991) Temperature and pressure of mylonitization in a Tertiary extensional shear zone, Ruby Mountains-East Humboldt Range, Nevada: Tectonic implications. Geology, 19, 82–86.

Jiang, W-T. and Peacor, D.R. (1993) Formation and modification of metastable intermediate sodium potassium mica, paragonite and muscovite in hydrothermally altered metabasites from northern Wales. American Mineralogist, 78, 782–793.

Kudoh, Y., Finger, L.W., Hazen, R.M., Prewitt, C.T., Kanzaki, M., and Veblen, D.R. (1993) Phase E: A high pressure hydrous silicate with unique crystal chemistry. Physics and Chemistry of Minerals, 19, 357–360.

Livi, K.J.T. and Veblen, D.R. (1987) "Eastonite" from Easton, Pennsylvania: A mixture of phlogopite and a new form of serpentine. American Mineralogist, 72, 113–125.

Livi, K.J., Veblen, D.R., Ferry, J.M., and Frey, M. (1997) Evolution of 2:1 layered silicates in low-grade metamorphosed Liassic shales of Central Switzerland. Journal of Metamorphic Geology, 15, 323–344.

Lister, G.S. and Snoke, A.W. (1984) S-C Mylonites. Journal of Structural Geology, 6, 617–638.

Merriman, R.J., Roberts, B., Peacor, D.R., and Hirons, S.R. (1995) Strain-related differences in the crystal growth of white mica and chlorite: a TEM and XRD study of the development of metapelitic microfabrics in the Southern Uplands thrust terrane, Scotland. Journal of Metamorphic Geology, 13, 559–576.

Page, R.H. (1980) Partial interlayers in phyllosilicates studied by transmission electron microscopy. Contributions to Mineralogy and Petrology, 75, 309–314.

Shau, Y-H. and Peacor, D.R. (1992) Phyllosilicates in hydrothermally altered basalts from DSDP Hole 504B, Leg 83—a TEM and AEM study. Contributions to Mineralogy and Petrology, 112, 119–133.

MANUSCRIPT RECEIVED JUNE 12, 1998
MANUSCRIPT ACCEPTED JULY 10, 1999
PAPER HANDLED BY PETER R. BUSECK